Contrib Mineral Petrol (2007) 153:321–337
DOI 10.1007/s00410-006-0149-5

ORIGINAL PAPER

Petrogenesis of the Pt–Pd mineralized Jinbaoshan ultramafic intrusion in the Permian Emeishan Large Igneous Province, SW China

Yan Tao · Chusi Li · Ruizhong Hu · Edward M. Ripley · Andao Du · Hong Zhong

Received: 13 January 2006 / Accepted: 4 October 2006 / Published online: 3 November 2006

Abstract The Jinbaoshan ultramafic intrusion is a sheet-like body with a thick wehrlite unit in the center and thin pyroxenite units at the margins. PGE are enriched in several disseminated sulfide zones in the intrusion. Olivine from the intrusion has low Fo and depleted Ni contents compared to olivine from coeval Emeishan picrites. Whole rock major and trace element concentrations suggest that the Jinbaoshan wehrlites originally contained <30% trapped liquid. The total amount of sulfide in the rocks exceeds that which could have been dissolved in the trapped liquid. The Jinbaoshan wehrlites are interpreted to represent residual assemblages formed by dissolution of plagioclase by passing magma. No clear evidence of crustal contamination is indicated by S, Nd and Os isotopes. We envision that sulfide saturation occurred at depth due to olivine and chromite crystallization. Immiscible sulfide droplets were transported to the Jinbaoshan conduit where they accumulated and reacted with magma successively passing through the conduit to achieve high PGE concentrations.

Keywords Wehrlite · Olivine · Sulfide · Platinum-group elements · Isotopes · Melt/rock reaction

Communicated by T.L. Grove.

Y. Tao · R. Hu · H. Zhong
State Key Laboratory of Ore Deposit Geochemistry, Institute of Geochemistry, Chinese Academy of Sciences, Guiyang 550002, China

C. Li (✉) · E. M. Ripley
Department of Geological Sciences, Indiana University, Bloomington, IN 47405, USA
e-mail: cli@indiana.edu

A. Du
National Research Center of Geoanalysis, Chinese Academy of Geological Sciences, Beijing 100037, China

Introduction

The Emeishan Large Igneous Province (ELIP) in southwest China is currently attracting considerable attention from several international mining companies who are looking for Pt–Pd deposits. In this region (Fig. 1), numerous mafic-ultramafic intrusions are spatially and temporally associated with the Permian Emeishan continental flood basalts that cover an area $>3 \times 10^5$ km^2 (Chung and Jahn 1995; Song et al. 2001; Xu et al. 2001, 2004; Xiao et al. 2004). Two types of mineral deposits are associated with the intrusions: Ni–Cu–PGE sulfide deposits in relatively small intrusions of broadly ultramafic composition, and Fe–Ti–V oxide deposits in relatively large intrusions of broadly mafic composition. The association of different types of mineralization with different types of rock is similar to that in the Bushveld Complex in South Africa. However, the field relations in these two magmatic systems are different. In the Bushveld Complex the two types of mineralization occur at different stratigraphic levels whereas in the ELIP they are hosted by separate intrusions. This difference suggests the presence of magma pluming systems composed of staging chambers and dynamic conduits in the ELIP. The Jinbaoshan ultamafic intrusion hosts the only known

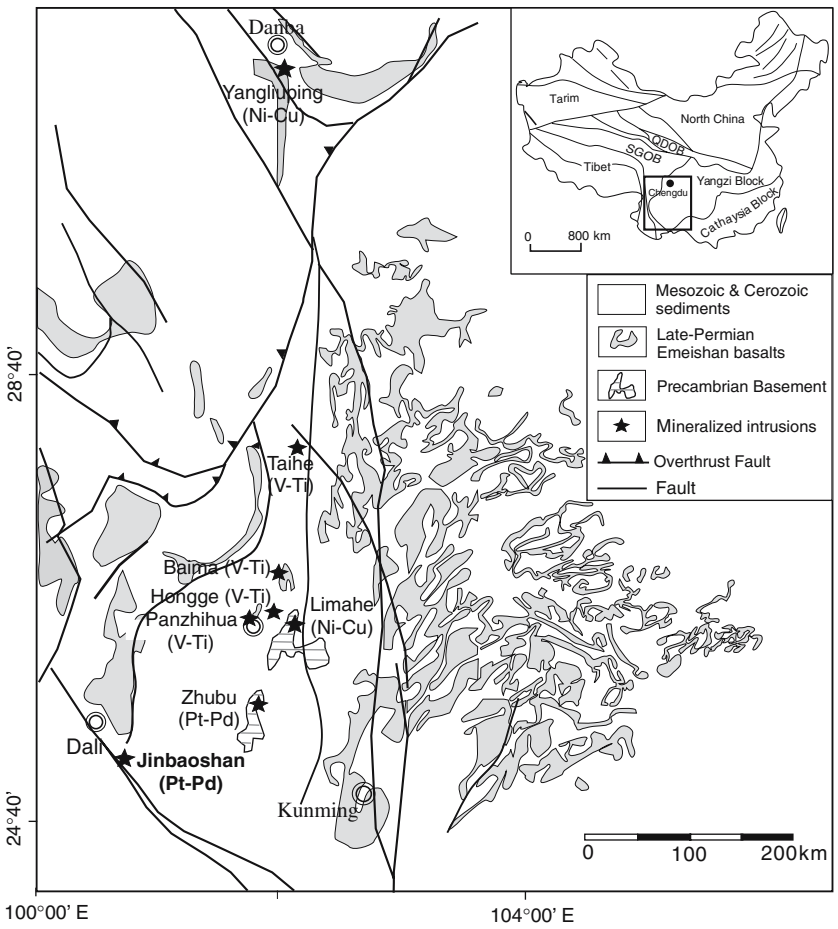

Fig. 1 Distribution of the Emeishan continental flood basalts and contemporaneous mafic-ultramfic intrusions in SW China (modified from Song et al. 2001)

economic Pt–Pd deposit in the province. It provides a window to study the evolution of magma and the processes of Pt–Pd enrichment in dynamic conduits. A better understanding of ore genesis in the Jinbaoshan intrusion is important for the on-going mineral exploration in the region.

Geological background

The Jinbaoshan intrusion is one of numerous mafic-ultramafic intrusions that are spatially and temporally associated with the late Permian Emeishan continental flood basalts in southwest China (Fig. 1). The Emeishan volcanic succession ranges from several hundred meters to 5 km in thickness. It unconformably overlies an early Late Permian carbonate formation and is covered by Triassic sedimentary sequences. The composition of the Emeishan volcanic succession varies from picrites and theoleiitic basalts to basaltic andesites (Chung and Jahn 1995; Song et al. 2001; Xu et al. 2001, 2004; Xiao et al. 2004). Geological relations indicate that the eruption of the Emeishan flood basalts took place at the end of the Guadalupian (~260 Ma) (Yin et al. 1992; Jin and Shang 2000). Due to post-eruption alteration and metamorphism of greenschist grade, Ar–Ar dating of whole rock samples of the Emeishan basalts (Boven et al. 2002; Ali et al. 2004; Fan et al. 2004) gives ages that are younger than the zircon U–Pb SHRIMP ages of 259–260 Ma for several coeval intrusions (Zhou et al. 2002a, 2005; Guo et al. 2004; Wang et al. 2006).

The Emeishan basalts and associated mafic-ultramafic intrusions together are referred to as the Emeishan Large Igneous Province (ELIP). The ELIP straddles the ~810 Ma subduction zone (Zhou et al. 2002b, 2006), which separates the Yangtze block to the east and the Songpan-Ganze Terrance to the west (Fig. 1). The Songpan-Ganze Terrance was part of the subducting oceanic lithosphere and the Yantze Block was the margin of the overriding supercontinent during Neoproterozoic time (Zhou et al. 2006). The easternmost part of the Songpan-Ganze Terrance is covered by a Late Triassic deep marine sedimentary sequence up to 10 km or more in thickness in many places (Burchfiel et al. 1995). The Yangtze Block comprises a

lower sequence of Late Mesoproterozoic to Triassic marine sediments, and an upper sequence of Jurassic and younger terrestrial basin deposits.

Significant uplift and erosion in the ELIP as a result of the Cenozoic India–Eurasia collision exposed numerous mafic-ultramafic intrusions that intruded in Precambrian basement. Some of these intrusions host important Fe–Ti–V oxide, Ni–Cu sulfide or Pt–Pd deposits (Fig. 1). Three largest Fe–Ti–V oxide deposits in the region are the Hongge (4572 Mt ore reserves), Baima (1,497 Mt ore reserves) and Panzhihua (1,333 Mt ore reserves) (Ma et al. 2003). These deposits are hosted by gabbroic intrusions. The Hongge and Panzhihua deposits were studied by Zhong et al. (2002, 2003) and Zhou et al. (2005), respectively. Three most important Ni–Cu sulfide deposits in the region are Limahe, Baimazhai and Yangliuping. They are hosted by mafic-ultramafic intrusions. The Yangliuping and Baimazhai deposits were described by Song et al. (2003) and Wang et al. (2006), respectively. Small scale mining activity ceased in 1992 at Limahe but is still active at Baimazhai. Pt–Pd mineralization has been found in several mafic-ultramafic intrusions including the Jinbaoshan and Zhubu intrusions, but the Jinbaoshan intrusion is the only one that contains economic Pt–Pd ore. Except a report on chromite chemistry by Wang et al. (2005), no publications in English have been given for the Jinbaoshan deposit.

The Jinbaoshan ultramafic intrusion is located in the western margin of the Yangtze Block (Fig. 1). The intrusion is a sheet-like body intruded into the Devonian dolomite that unconformably overlies the Proterozoic metamorphic rocks. The Jinbaoshan intrusion is exposed in an area measuring ~5 km long and ~1 km wide (Fig. 2a). The southern and northern parts of the Jinbaoshan intrusion were partially eroded prior to the Triassic era and were then covered by Triassic sediments. The middle part of the intrusion was eroded by the Lishe River. The thickness of the intrusion varies from 20 to 150 m (Fig. 2b, c). The Jinbaoshan ultramafic intrusion is essentially a wehrlite body. Minor hornblende pyroxenite (<10%) is present in the margins of the intrusion in some places. The intrusive relation between the Jinbaoshan werhlite and associated gabbroic rocks is indicated in cross sections (Fig. 2c). Wang et al. (2005) excluded the gabbroic rocks from the Jinbaoshan ultramafic intrusion. However, Yang (1989) thought that the gabbroic rocks are parts of the Jinbaoshan intrusion. In this paper we will evaluate the contradictory interpretations using mineral and chemical analyses.

The textures and modal compositions of silicate minerals in the Jinbaoshan wehrlites are generally homogeneous. A sub-horizontal layer containing 5–12 vol% chromite with a thickness ranging from 5 to 15 m occurs in the middle part of the wehrlite unit. Except for the chromite layer and disseminated sulfide zones within the wehrlite unit there is no visible igneous layering in the intrusion. Marble hornfels (<0.5 m thick) occur in the contact with dolomites in some places.

On-going exploration at Jinbaoshan has delineated ores containing ~45 tons of Pt + Pd. The concentrations of Pt + Pd in the ores vary mostly from 1 to 5 ppm and rarely up to 17 ppm. The enrichment of Pt and Pd is spatially associated with disseminated sulfide (<3 vol%) that occurs as discontinuous layers within the wehrlite unit. The thickness of an individual disseminated sulfide layer varies from several centimeters to a couple of meters.

Petrography

A total of 25 samples from the Jinbaoshan ultramafic intrusion and associated gabbroic rocks were collected from outcrops and adits. The relative positions of the samples are shown in Fig. 3.

Typical gabbro from Jinbaoshan comprises >60 vol% tabular plagioclase and ~30 vol% granular augite and minor hornblende, biotite and magnetite. Plagioclase has a tabular shape averaging ~ 1 × 3 mm. Augite crystals are mostly <1 mm across. Most augite crystals are altered to tremolite and talc whereas most plagioclase crystals are altered to chlorite plus Fe-rich epidote containing up to 13 wt% Fe. Small calcite veins are present in microfractures in the rocks.

Chromite in the chromite-rich layer in the werhlite unit is characterized by a ring shape formed by several connected subhedral chromite crystals surrounding an olivine crystal. The diameters of individual chromite rings vary from several millimeters to several centimeters in thin sections. The margins of chromite grains are altered to an Fe-rich variety. Secondary magnetite veins are present in microfractures in chromites.

Wehrlite contains 40–70 vol% olivine, 10–20 vol% clinopyroxene and minor chromite, plagioclase and primary hornblende and phlogopite. Olivine crystals are euhedral to subhedral and vary in size from 0.5 to 3 mm in diameter. Olivine inclusions in clinopyroxene tend to be smaller than isolated grains and are commonly characterized by a rounded shape (Fig. 4a). Clinopyroxene commonly occurs as large poikilitic crystals (up to 1 cm in diameter) containing olivine and chromite inclusions. Hornblende commonly forms a reaction rim surrounding clinopyroxene. Phlogopite and plagioclase occur in the interstitial spaces. Most

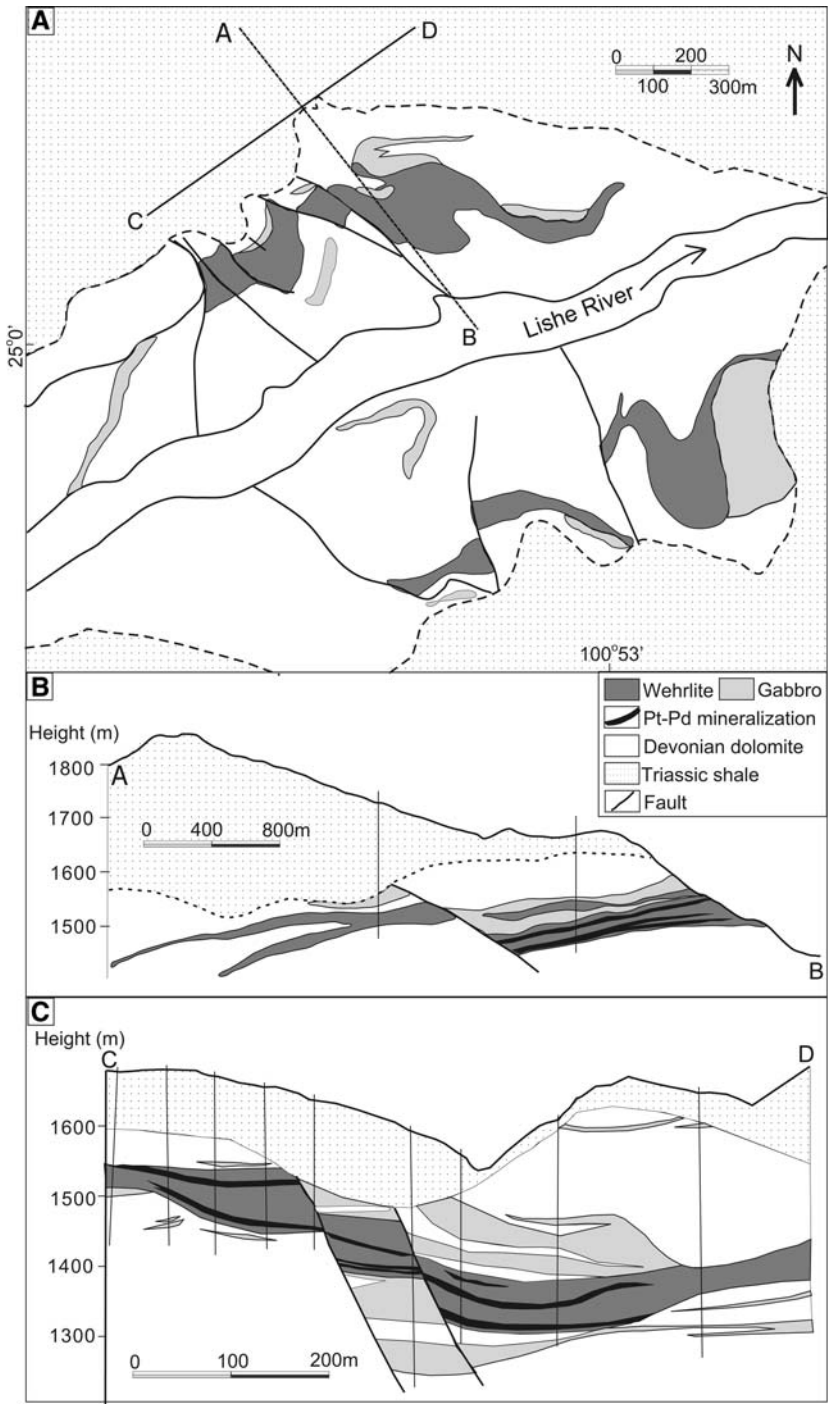

Fig. 2 Geological map and sections of the Jinbaoshan intrusion (modified from Yang 1989)

olivine crystals in the rocks are completely altered to serpentine plus magnetite.

Hornblende pyroxenite contains >50 vol% augite, 10–30 vol% hornblende and minor biotite and magnetite. Augite occurs as euhedral crystals 3–8 mm across. Smaller augite grains occur as inclusions in poikilitic hornblende. Most augite crysals are altered to actinolite and talc.

Primary sulfide minerals are pyrrhotite, pentlandite and chalcopyrite. They occur in the interstitial spaces in wehrlites. The primary sulfide assemblages are commonly altered to magnetite, pyrite and millerite (Fig. 4b). Local redistribution of sulfides is indicated by the presence of calcite–sulfide veins (chalcopyrite, pyrite and millerite) in microfractures in the rocks.

Platinum-group minerals (PGM) are present in sulfide-mineralized wehrlites. They include moncheite ($PtTe_2$) (10 grains), sperrylite ($PtAs_2$) (3 grains), a Pt–Fe alloy with composition close to tetraferroplatinum (PtFe) and a rustenburgite (Pt_3Sn). Four grains of

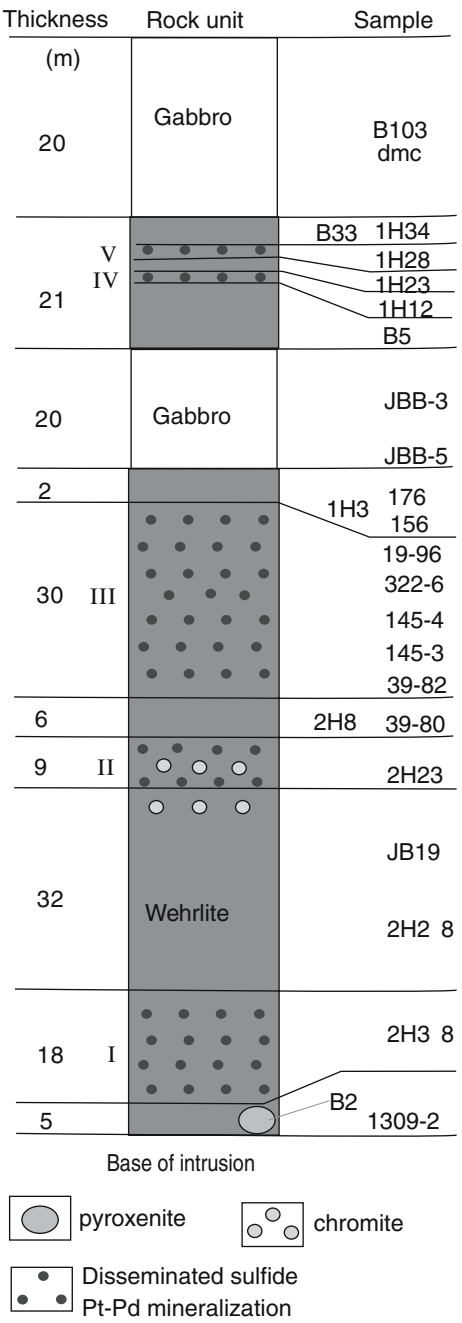

Fig. 3 A composite stratigraphic column showing sample locations

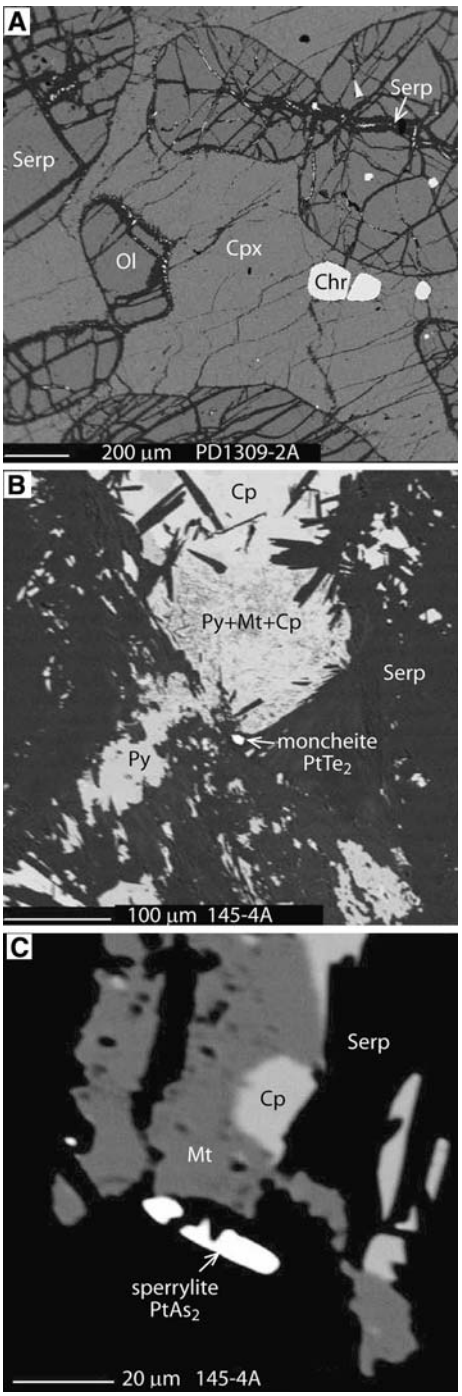

Fig. 4 Back scattered electron images showing **a** olivine inclusions in clinopyroxene in wehrlite, **b** a Pt telluride associated with altered sulfide assemblage in wehrlite, and **c** a Pt arsenide associated with secondary magnetite in wehrlite. *Ol* olivine, *Cpx* clinopyroxene, *Chr* chromite, *Serp* serpentine, *Mt* magnetite, *Cp* chalcopyrite, *Py* pyrite

native gold are also found in the samples. The sizes of the PGM vary between 10 and 20 µm. They are closely associated with altered sulfide assemblages (Fig. 4b, c).

Analytical methods

Mineral chemical compositions were determined by wavelength-dispersive X-ray analysis at 15 kV using a CAMECA SX50 electron microprobe at Indiana University. Major elements in minerals were analyzed using a 1 µm beam with a beam current of 20 nA and a counting time of 20 s. Trace elements (Ni and Ti in

silicates, and Pd in pentlandite) were analyzed using a beam current of 100 nA and a peak counting time of 50 s. The detection limits for these elements under such conditions are 120 ppm Ni, 70 ppm Ti and 200 ppm Pd. Raw data were corrected using the PAP program supplied by CAMECA. Analytical reproducibility was within 2%. The accuracy of the analyses was monitored using reference materials.

Whole rock major element compositions were analyzed by wet chemistry. The concentrations of S in the samples were determined by the Leco induction furnace-titration technique. Whole rock trace element compositions (including Ni and Cu) were analyzed by ICP-MS. The analytical procedures, detection limits and precision are given in Qi and Grégoire (2000). The concentrations of PGE in whole rock samples were determined by the combination of NiS bead pre-concentration, Te co-precipitation and ICP-MS analysis. The analytical procedures, detection limits and precision are given in Qi et al. (2003). All of the whole rock chemical analyses were carried out in the Institute of Geochemistry, Chinese Academy of Sciences, Guiyang, China.

The concentrations of Sm and Nd and their isotope ratios were determined using a VG-354 thermal ionization magnetic sector mass spectrometer in the Institute of Geology and Geophysics, Chinese Academy of Sciences, Beijing. The details of the method are given in Zhang et al. (2001). Mass fractionation correction for Nd isotopic ratios was based on $^{146}Nd/^{144}Nd$ of 0.7219. Uncertainties in Sm/Nd ratio is less than ±0.5% relative. The concentrations of Re and Os and their isotopic ratios were determined using a VG Plasma Quad ICP-MS in the National Research Center of Geoanalysis in Beijing. The analytical procedures are similar to those of Shirey and Walker (1995) and Du et al. (2004).

Sulfide mineral separates were analyzed for S isotopic compositions using elemental analyzer-continuous flow isotope ratio mass spectrometry (Studley et al. 2002) at Indiana University. Sample powders were placed in tin cups with 1–1.5 mg of V_2O_5 and combusted at ~1,800°C, with a reactor column temperature of 1,010°C. Analyses of SO_2 were made using a Finnigan MAT 252 stable isotope ratio mass spectrometer, with results reported in standard delta notation relative to V-CDT. Analytical uncertainty was less than ±0.05‰, and sample reproducibility was within ±0.3‰. Sulfide standards utilized included IAEA S-1 (with a defined value of –0.3‰ V-CDT), IAEA S-2 (21.7‰), IAEA S-3 (–31.3‰) and several Indiana University laboratory standards.

Results

Mineral chemistry

The compositions of the PGM are listed in Table 1. The compositions of chromites from the Jinbaoshan ultramafic intrusion are given in Wang et al. (2005). Representative analyses of olivine and augite from the Jinbaoshan ultramafic intrusion are listed in Table 2. Olivine has restricted Fo contents ranging between 82.6 and 83.6 mole%. The concentrations of Ni in olivine vary between 1,600 and 2,000 ppm. Olivine from the Jinbaoshan ultramafic intrusion is depleted in Ni compared to olivine with similar Fo contents from the Emeishan picrites given by Xu and Chung (2001) (<2,000 vs. ~2,500 ppm). Most olivine phenocrysts from the Emeishan picrites contain higher Fo than olivine from the Jinbaoshan intrusion.

Augite from the wehrlite unit of the Jinbaoshan ultramafic intrusion has higher Mg# and higher Cr and

Table 1 Compositions of platinum-group minerals from the Jinbaoshan deposit

Mineral Formula	Sperrylite $PtAs_2$	Moncheite $PtTe_2$	Rustenburgite Pt_3Sn	Tetraferroplatinum PtFe
Pt	58.96	38.76	73.57	78.67
Pd	0.03	0.54	6.80	0.06
Fe	1.00	0.28	0.88	14.38
Co	0.04	0.00	0.00	0.03
Ni	0.00	0.06	0.01	1.64
Cu	0.07	0.00	0.17	4.15
As	39.55	0.00	0.00	0.21
S	0.00	0.00	0.04	0.00
Bi	0.00	9.15	0.00	0.00
Sb	0.08	0.42	0.00	0.04
Te	0.01	50.25	0.21	0.00
Sn	0.00	0.00	18.30	0.00
Total (wt%)	99.74	99.44	99.98	99.17

Table 2 Representative analyses of olivine and clinopyroxene from the Jinbaoshan intrusion and associated gabbro

Sample	Olivine in wehrlite									Sample	Cpx in wehrlite		Cpx in gabbro	
	1309-2	1309-2	1309-2	1309-2	1309-2	JB19	JB19	JB19	JB19		2H22	2H22	JBB-3	JBB-3
SiO_2	39.64	39.52	39.56	39.35	39.23	39.57	39.32	39.23	39.34	SiO_2	51.24	51.47	51.64	53.43
FeO	15.91	15.90	16.13	16.02	16.28	15.71	15.65	15.60	15.75	TiO_2	0.59	0.63	1.00	1.04
MnO	0.26	0.30	0.21	0.26	0.26	0.22	0.23	0.21	0.25	Al_2O_3	3.01	3.02	2.12	2.40
MgO	43.87	43.96	43.78	43.87	44.00	44.04	44.07	44.22	44.05	Cr_2O_3	0.96	0.94	0.08	0.29
NiO	0.23	0.23	0.23	0.23	0.23	0.23	0.22	0.23	0.22	FeO	5.47	5.23	9.58	9.04
CaO	0.12	0.14	0.11	0.11	0.11	0.10	0.09	0.09	0.11	MnO	0.17	0.15	0.21	0.20
Total (wt%)	100.0	100.0	100.0	99.8	100.1	99.9	99.6	99.6	99.7	MgO	17.17	16.92	15.08	14.99
Fo (mole%)	83.0	83.0	82.8	82.9	82.7	83.3	83.3	83.4	83.2	CaO	20.65	20.76	19.00	17.75
Ni (ppm)	1824	1792	1800	1784	1808	1824	1729	1824	1753	Na_2O	0.32	0.32	0.29	0.26
										Total (wt%)	99.59	99.44	99.00	99.39

lower Ti contents than augite from the Jinbaoshan gabbros (Fig. 5a, b). The Cr_2O_3 and TiO_2 contents of augite from the wehrlite units are from 0.85 to 1 wt% and from 0.5 to 0.9 wt%, respectively. The Cr_2O_3 and TiO_2 contents of augite from the Jinbaoshan gabbros are <0.3 wt% and from 0.9 to 1.2 wt%, respectively.

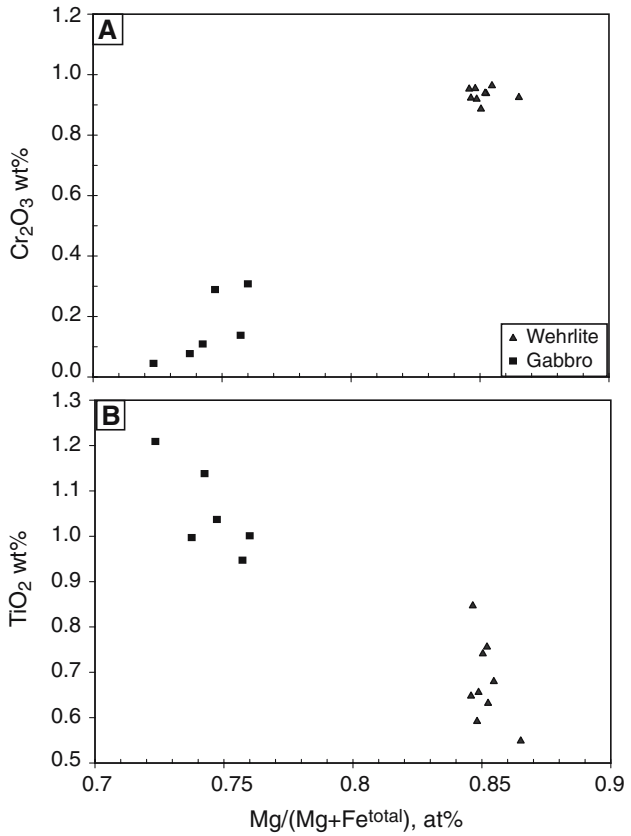

Fig. 5 Comparison of Mg-number and Cr_2O_3 and TiO_2 contents in clinopyroxenes

Two nickel sulfide minerals, pentlandite ($Fe_4Ni_5S_8$) and millerite (NiS), contain trace amounts of Pd. The concentrations of Pd in pentlandite and millerite vary between 500 and 1,700 ppm, and between 1,100 and 1,900 ppm, respectively (Fig. 6).

Major elements

Whole rock major and trace element compositions are listed in Table 3. The amounts of total Fe in whole rocks are reported as FeO*. The samples analyzed are variably altered and therefore have variable loss-on-ignition (LOI). For comparison we have normalized the whole rock raw data to anhydrous compositions by correcting for LOI. We use the normalized values for the discussions below. The data of Yang (1989) are included in our comparison

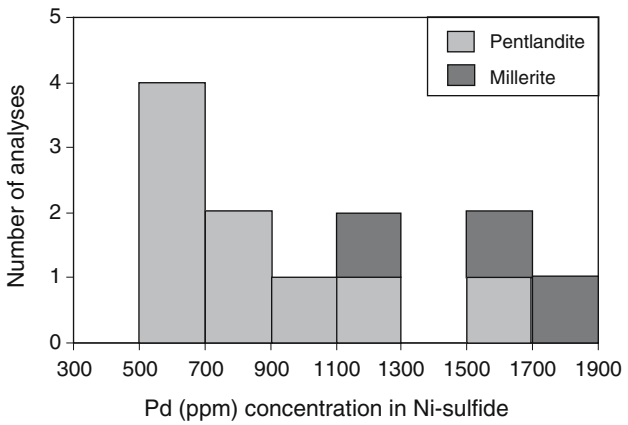

Fig. 6 Variations of Pd concentrations in pentlandite and millerite

Table 3 Major, trace and chalcophile element concentrations in whole rocks from the Jinbaoshan intrusion and associated gabbro

Sample	2H23	2H28	2H38	1H28	1H20	1H12	322-6R	145-3R	145-4R	JB19	19–96	39–82	B2
Rock type	PGE-enriched wehrlite												Pyroxenite
Oxide (wt%)													
SiO_2	35.93	38.38	35.03	32.86	36.93	32.37	34.57	39.63	35.3	39.07	38.16	37.54	43.78
TiO_2	1.14	0.44	0.42	0.49	0.35	0.24	0.47	0.40	0.41	0.55	0.46	0.42	0.84
Al_2O_3	6.90	5.07	4.91	3.06	3.21	2.75	4.48	1.41	4.25	4.01	2.91	2.02	11.32
FeO^{total}	14.12	12.81	16.01	14.44	13.66	15.13	8.43	9.98	12.22	10.96	10.34	8.17	8.23
MnO	0.12	0.17	0.13	0.16	0.17	0.09	0.12	0.11	0.10	0.16	0.15	0.15	0.13
MgO	25.05	28.30	27.57	33.34	32.65	31.05	27.4	31.2	31.6	31.1	32.18	32.51	18.42
CaO	2.93	4.16	2.25	2.48	0.35	3.73	5.8	0.8	0.6	2.0	4.13	7.4	10.85
Na_2O	0.29	0.19	0.20	0.08	0.07	0.08	0.12	0.11	0.09	0.21	0.1	0.035	0.36
K_2O	0.70	0.14	0.26	0.12	0.17	0.09	0.11	0.09	0.06	0.18	0.16	0.071	0.37
P_2O_5	0.04	0.03	0.03	0.03	0.03	0.03	0.15	0.13	0.30	0.20	0.069	0.072	0.06
Cr_2O_3	4.33	2.05	0.51	0.81	0.66	0.60	0.69	0.90	0.83	0.77	1.06	0.96	0.18
S	1.43	0.20	1.08	1.07	0.50	1.13	0.42	0.74	1.79	0.60	0.24	0.76	0.21
LOI	6.89	8.17	11.54	10.84	11.48	12.67	16.92	13.93	11.65	9.59	10.10	9.70	4.74
Total	99.87	100.09	99.94	99.77	100.21	99.98	99.68	99.43	99.21	99.41	100.05	99.81	99.49
Mg#	0.76	0.80	0.75	0.80	0.81	0.79	0.85	0.85	0.82	0.84	0.85	0.88	0.80
Trace element (ppm)													
Ni	3079	1559	2396	1659	2344	2745	1344	4570	4555	1332	1912	3329	734
Cu	2123	405	960	3545	767	4341	411	944	5046	9	29	1888	433
Co	178	154	203	151	192	179	143	229	269	196	133	189	103
Rb	28.5	2.0	8.1	3.1	4.3	0.9	4.9	3.3	1.9	5.9	6.5	3.4	12.3
Ba	179.2	22.2	59.5	18.6	35.1	6.1	31.3	22.1	15.5	87.9	48.3	19.4	70.6
Th	2.13	0.28	0.93	1.44	0.62	0.46	0.78	0.80	0.60	0.96	0.95	0.71	1.54
U	0.48	0.07	0.35	0.31	0.14	0.23	0.18	0.20	0.36	0.22	0.23	0.19	0.46
Nb	10.36	1.21	3.46	6.42	2.88	1.99	3.40	3.51	2.84	5.06	4.43	4.07	11.20
Ta	0.72	0.08	0.24	0.38	0.18	0.13	0.21	0.22	0.17	0.31	0.30	0.28	0.67
Zr	84.6	13.5	20.0	55.7	24.0	17.7	26.7	29.1	22.7	38.3	37.6	31.0	89.4
Hf	2.65	0.85	0.62	1.46	0.78	0.52	0.85	0.96	0.58	1.18	1.37	1.13	2.60
Sr	60.8	23.6	53.5	19.2	6.7	54.4	126.0	10.0	7.6	29.5	15.7	7.5	134.0
Y	10.51	4.78	5.40	5.66	3.44	2.79	3.99	2.98	2.66	5.77	5.03	4.10	12.68
La	12.68	2.06	6.78	5.30	4.06	2.86	4.65	4.01	3.22	5.70	5.06	4.34	11.49
Ce	28.0	5.0	13.2	11.6	8.9	6.0	9.7	8.5	6.8	13.1	12.5	10.2	27.5
Pr	3.49	0.70	1.55	1.48	1.12	0.73	1.17	0.98	0.77	1.56	1.36	1.05	3.05
Nd	14.30	3.34	6.56	6.65	5.15	3.39	4.32	4.01	3.20	6.93	5.14	3.45	12.07
Sm	2.92	0.99	1.36	1.31	0.95	0.66	0.90	0.82	0.74	1.55	1.40	1.01	2.90
Eu	0.82	0.27	0.42	0.39	0.20	0.19	0.25	0.13	0.10	0.40	0.36	0.23	0.76
Gd	2.91	1.18	1.39	1.39	1.06	0.64	0.92	0.76	0.64	1.34	1.24	0.96	2.84
Tb	0.41	0.18	0.22	0.20	0.13	0.10	0.13	0.12	0.09	0.20	0.19	0.15	0.43
Dy	2.18	1.04	1.19	1.16	0.69	0.60	0.72	0.60	0.54	1.06	1.09	0.87	2.54
Ho	0.43	0.21	0.22	0.24	0.14	0.10	0.16	0.12	0.10	0.20	0.22	0.17	0.49
Er	1.14	0.55	0.59	0.60	0.40	0.26	0.38	0.28	0.31	0.59	0.58	0.43	1.36
Tm	0.16	0.06	0.07	0.09	0.06	0.04	0.05	0.04	0.04	0.10	0.07	0.07	0.18
Yb	1.08	0.49	0.46	0.58	0.35	0.28	0.44	0.35	0.27	0.58	0.59	0.44	1.22
Lu	0.14	0.07	0.07	0.08	0.05	0.04	0.05	0.05	0.04	0.07	0.08	0.06	0.18
Platinum-group element (ppb)													
Os	61	10	15	34	35	54					54	172	1.3
Ir	134	21	52	79	56	113	185	480	350	20	71	283	2.6
Ru	31	7	10	25	19	30	69	223	162	8	26	87	0.7
Rh	124	18	41	52	33	67	131	332	302	13	45	221	1.6
Pt	2008	190	557	564	795	1683	3672	6383	6430	338	967	3661	20
Pd	3724	351	1216	640	852	1990	6305	10080	10240	462	1089	5836	40

Sample	1H34	1H23	1H3	19-176	1309-2	B33	B5	19-156	39-80	2H8-2	JBB-3	JBB-5	B103	DMC
Rock unit	Wehrlite										Gabbro			
Oxide (wt%)														
SiO_2	35.25	38.24	37.78	37.73	38.22	38.7	39.13	38.32	38.06	36.86	47.76	42.89	45.59	41.35
TiO_2	0.34	0.37	0.40	0.70	0.62	0.47	0.83	0.53	0.38	0.37	2.90	1.67	2.65	2.40
Al_2O_3	2.46	3.46	3.37	3.30	7.55	5.90	2.91	2.92	2.39	3.92	16.14	15.4	16.86	13.74
FeO^{total}	14.55	11.15	11.81	8.42	11.62	11.71	11.74	13.14	10.67	12.95	13.88	11.26	11.79	7.35

Table 3 continued

Sample	1H34	1H23	1H3	19-176	1309-2	B33	B5	19-156	39-80	2H8-2	JBB-3	JBB-5	B103	DMC
Rock unit	Wehrlite										Gabbro			
MnO	0.14	0.13	0.09	0.14	0.18	0.13	0.18	0.15	0.14	0.11	0.15	0.14	0.14	0.19
MgO	32.20	32.53	32.56	32.6	29	28.6	28.74	29.61	30.7	31.03	4.95	5.83	5	4.98
CaO	1.63	0.95	1.15	2.5	2.6	1.8	5.26	3.26	5.64	1.66	6.04	8.24	8.1	16.57
Na_2O	0.08	0.08	0.13	0.18	0.27	0.18	0.091	0.1	0.065	0.11	3.66	2.09	1.89	2.07
K_2O	0.08	0.15	0.22	0.17	0.32	0.15	0.11	0.14	0.18	0.21	0.33	0.14	0.39	0.38
P_2O_5	0.03	0.03	0.03	0.2	0.27	0.17	0.15	0.074	0.087	0.03	0.3	0.2	0.063	0.078
Cr_2O_3	0.70	0.72	1.07	0.85	1.03	0.84	0.82	0.99	1.04	0.74	0.03	0.03	0.02	0.01
S	0.17	0.16	0.09	0.72	0.30	0.21		0.13	0.11	0.10				
LOI	12.45	11.93	11.25	12.21	7.90	10.53	9.31	10.01	10.31	11.94	3.38	12.02	7.42	10.53
Total	100.06	99.91	99.95	99.72	99.88	99.39	99.31	99.38	99.77	100.03	99.52	99.91	99.91	99.65
Mg#	0.80	0.84	0.83	0.87	0.82	0.81	0.81	0.80	0.84	0.81	0.39	0.48	0.43	0.55
Trace element (ppm)														
Ni	1514	1382	1354	1545	1295	1306	1135	1470	1337	1371	105	132	52	47
Cu	212	19	8	64	41	9	46	68	12	21	173	67	43	45
Co	404	144	115	134	190	135	136	151	137	148	41	38	63	48
Rb	3.5	3.8	5.9	6.8	11.7	6.5	3.8	6.7	5.7	6.6	7.8	3.8	18.1	17.5
Ba	27.7	27.0	35.6	47.5	105.6	154.0	38.9	56.1	40.4	49.9	578.9	224.3	146.0	143.2
Th	0.65	0.70	0.67	1.10	0.98	0.95	0.58	1.06	0.83	0.70	1.64	4.36	3.20	2.93
U	0.15	0.15	0.15	0.29	0.20	0.26	0.13	0.26	0.19	0.21	0.50	1.69	0.80	0.81
Nb	2.78	3.30	3.17	6.65	4.94	4.10	3.17	5.07	3.75	3.05	14.87	13.88	25.04	22.25
Ta	0.22	0.22	0.21	0.39	0.32	0.28	0.19	0.32	0.23	0.20	0.94	0.88	1.42	1.24
Zr	25.5	28.6	28.5	45.6	42.0	35.3	26.7	38.7	30.9	26.6	167.6	139.0	179.5	156.0
Hf	4.24	0.82	0.83	1.39	1.30	1.09	1.00	1.38	1.26	0.92	4.50	3.68	5.15	4.39
Sr	22.3	10.2	18.3	41.4	86.9	21.3	16.7	21.3	15.3	45.2	521.9	391.6	492.2	560.3
Y	2.69	3.63	4.68	7.54	5.48	5.88	5.46	5.80	5.02	3.56	31.83	21.22	23.49	22.12
La	4.06	3.85	6.86	6.77	6.35	5.15	3.58	5.52	5.78	4.97	11.89	20.11	27.11	24.84
Ce	8.0	8.4	14.1	15.4	14.20	13.5	9.1	13.0	13.0	9.7	30.0	43.0	62.5	54.9
Pr	0.96	1.10	1.76	1.84	1.69	1.68	1.05	1.47	1.41	1.21	4.32	5.29	7.28	6.35
Nd	4.07	4.60	6.89	8.34	6.96	7.44	3.90	5.21	5.05	4.64	20.74	23.19	30.09	26.47
Sm	0.77	0.94	1.33	1.84	1.50	1.65	1.16	1.41	1.32	1.02	5.62	4.86	6.56	6.29
Eu	0.17	0.23	0.59	0.22	0.41	0.40	0.30	0.38	0.32	0.51	1.74	1.79	1.79	1.70
Gd	0.77	0.96	1.33	1.75	1.26	1.58	1.23	1.34	1.15	0.91	6.22	4.58	6.18	5.54
Tb	0.10	0.15	0.20	0.25	0.20	0.24	0.19	0.22	0.20	0.13	0.98	0.71	0.90	0.82
Dy	0.54	0.76	1.05	1.58	1.05	1.26	1.12	1.23	1.09	0.76	6.16	4.09	4.88	4.59
Ho	0.10	0.15	0.20	0.28	0.20	0.27	0.23	0.25	0.22	0.17	1.19	0.80	0.94	0.83
Er	0.33	0.42	0.53	0.84	0.62	0.57	0.62	0.65	0.59	0.46	3.07	2.16	2.48	2.32
Tm	0.05	0.05	0.08	0.10	0.08	0.09	0.08	0.10	0.09	0.05	0.44	0.31	0.34	0.29
Yb	0.27	0.38	0.51	0.79	0.52	0.59	0.54	0.59	0.54	0.47	2.83	1.94	2.10	1.96
Lu	0.04	0.06	0.06	0.09	0.08	0.06	0.08	0.09	0.08	0.06	0.41	0.26	0.29	0.25
Platinum-group element (ppb)														
Os	3.4	3.4	1.5					8.6	3.0	2.1				
Ir	7.6	6.7	3.5	7.5	7.1	2.5		8.9	5.0	6.1				
Ru	9.4	4.5	4.0	3.1	4.6	2.4		3.0	1.4	3.2				
Rh	3.8	3.3	2.6	4.3	7.1	1.0		5.8	3.8	4.4				
Pt	77	55	24	58	56	13.2		57	37	63				
Pd	58	46	31	103	81	22.1		63	43	76				

(Fig. 7a–c). The contents of MgO in the Jinbaoshan wehrlites vary between 27 and 38 wt%. The contents of MgO in the Jinbaoshan pyroxenites vary between 15 and 22 wt%. In contrast, the contents of MgO in the Jinbaoshan gabbros are much lower, varying between 5 and 9 wt%. There are compositional gaps between the rocks of the Jinbaoshan ultramafic intrusion and associated gabbros (Fig. 7a–c).

Trace elements

The trace element compositions of the Jinbaoshan ultramafic intrusion and associated gabbros are given in Table 3. The slopes of trace element patterns of the intrusive rocks are distinctly different from that of normal mid-ocean ridge basalts (N-MORB) but are rather similar to that of typical ocean island basalts

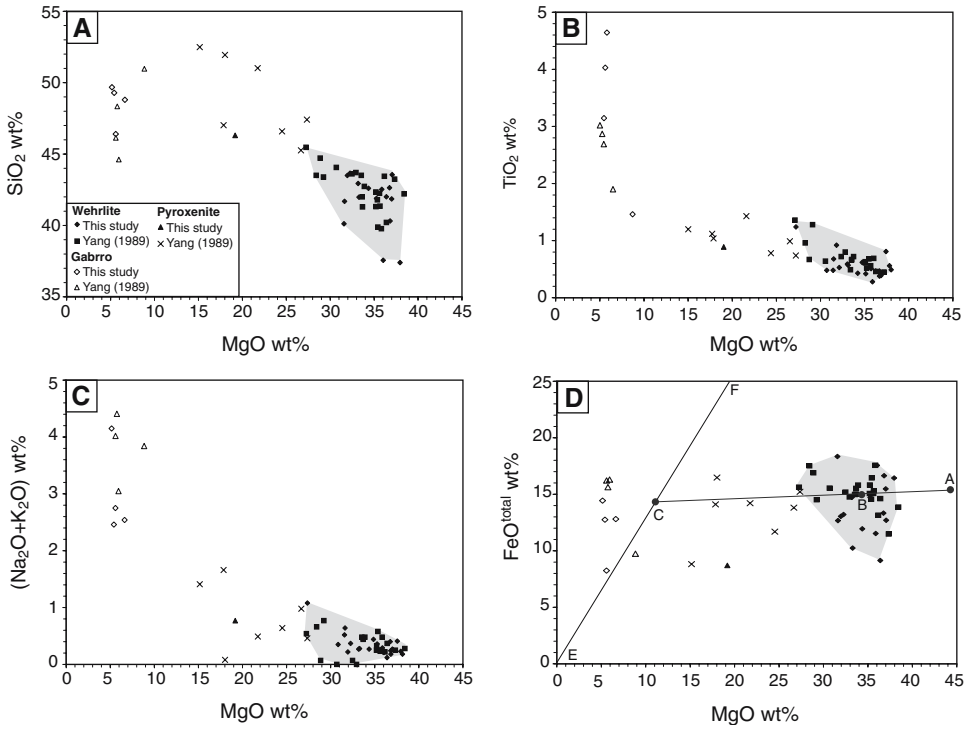

Fig. 7 Plots of MgO versus SiO_2 (**a**), TiO_2 (**b**), (Na_2O + K_2O) (**c**) and FeO^{total} (**d**) for the Jinbaoshan intrusive rocks and the Emeishan picrites. Point *A* is the composition of olivine Fo84. Point *B* is the average compositions of wehrlite samples from the Jinbaoshan intrusion. Line *E* to *F* represents the ratio of FeO/MgO = 1.16, which is 3.3 times the ratio of olivine Fo84. Point *C* is the estimated composition of trapped liquid for the Jinbaoshan wehrlites assuming that the rocks were originally mixtures of olivine Fo84 with coexisting liquid

(OIB) (Fig. 8a, b). However, the trace element patterns of the intrusive rocks from the Jinbaoshan intrusion are not as smooth as those of the basalts. Several elements such as Rb and Ba in the intrusive rocks are highly variable, possibly due to alteration. Sr and Eu show a significant negative anomaly in the Jinbaoshan wehrlites. No positive anomaly of Sr and Eu is present in the Jinbaoshan gabbros. The ratios of a highly incompatible over a less incompatible element such as Ce/Yb and Nb/Y of the Jinbaoshan wehrlites are similar to the values of OIB.

Ni, Cu, S and platinum group elements

The concentrations of Ni, Cu, S and PGE in the rocks of the Jinbaoshan ultramafic intrusion are given in Table 3. The contents of S in pyroxenite and wehrlites vary from 0.09 to 0.3 wt%. The contents of S in PGE-enriched wehrlites are significantly higher, varying between 0.24 and 1.8 wt%. Pyroxenites and wehrlites contain 13–77 ppb Pt and 22–103 ppb Pd. PGE-enriched wehrlites contain 0.3–6 ppm Pt and 0.5–10 ppm Pd. Correlations between individual PGE in the samples are good (Fig. 9a–f).

The primitive mantle-normalized PGE patterns of the Jinbaoshan wehrlite samples are illustrated in Fig. 10. Both sulfide-enriched and sulfide-poor wehrlites have similar patterns. They show moderate negative Ru anomaly and depletion in Ir, Ru and Rh relative to Pt and Pd.

Sulfur isotopes

Values of $\delta^{34}S$ for sulfide minerals are listed in Table 4. Disseminated pyrrhotite and chalcopyrite plus pyrite and chalcopyrite found as veins in the igneous rocks have a restricted range in $\delta^{34}S$ values from 0.6 to 2.8‰. The values are within the range of 0 ± 2‰ considered to be normal for sulfur of mantle derivation. In contrast, pyrite in dolomite footwall rocks and xenoliths, as well as that present as matrix in breccias composed of igneous rock fragments, is characterized by highly variable $\delta^{34}S$ values, ranging from –23 to 19‰.

Neodymium and osmium isotopes

The Nd isotopic compositions of rocks from the Jinbaoshan ultramafic intrusion and associated gabbro are

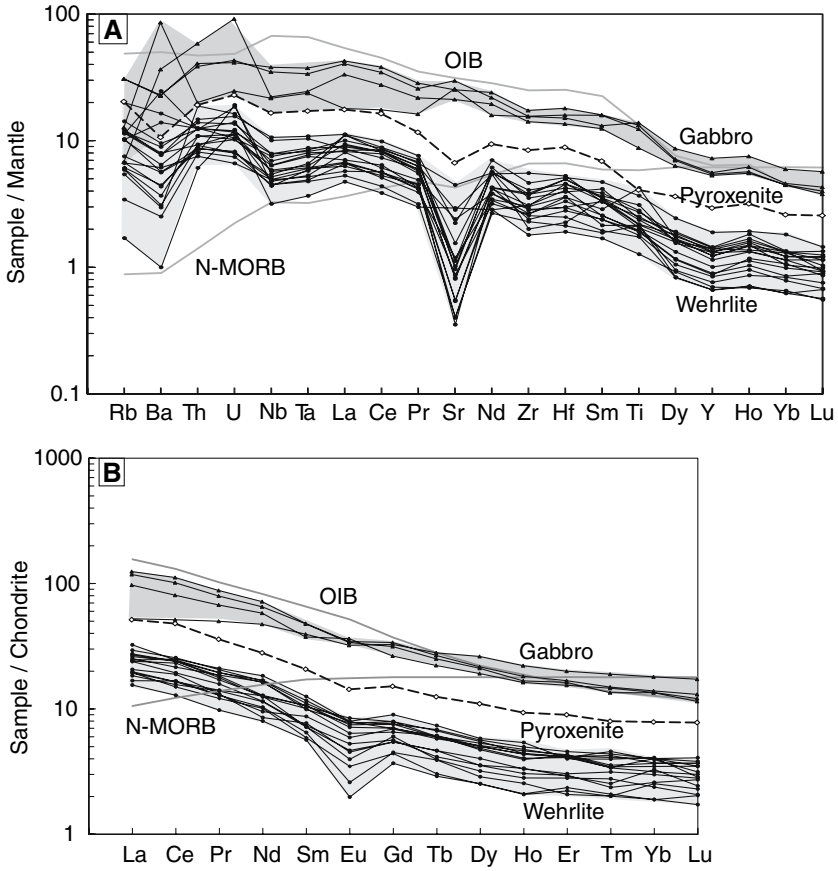

Fig. 8 **a** Primitive mantle-normalized trace element patterns for the Jinbaoshan intrusive rocks. The values for primitive mantle, typical oceanic basalt (*OIB*) and normal mid-ocean ridge basalt (*N-MORB*) are from Sun and McDonough (1989). **b** chondrite-normalized rare earth element patterns for the Jinbaoshan intrusive rocks and the Emeishan picrites. The chondrite values are from Anders and Grevesse (1989)

listed in Table 5. On a Sm–Nd isochron diagram (Fig. 11), the analyses do not form a 259 Ma isochron which corresponds to the possible age of the Jinbaoshan ultramafic intrusion (Zhou et al. 2002c). The wehrlite and pyroxenite samples cluster with $^{147}Sm/^{144}Nd$ values between 0.1231 and 0.1399 along a chondritic reference isochron. The values of ε_{Nd} at 259 Ma for these samples range from –0.05 to 0.81, indicating that they are near chondritic. The gabbro sample is characterized by a much higher $^{147}Sm/^{144}Nd$ value (0.171) and plots above the chondritic reference isochron at 259 Ma (Fig. 11). The value of ε_{Nd} at 259 Ma for the gabbro sample is 4.2, higher than that for the wehrlite and pyroxenite samples.

Three sulfide-poor wehrlite samples, two sulfide veins, and two sulfide-bearing wehrlite samples have been analyzed for Os isotopic composition (Table 6). Rhenium and Os are positively correlated (Fig. 12) and Re/Os values are relatively low, with ratios less than 0.3. On a Re–Os isochron diagram the samples are suprachondritic and do not form a 259 Ma isochron (Fig. 13). Values of γ_{Os} (259 Ma) range from ~22 to 81, with no distinction between sulfide-rich and sulfide-poor samples.

Discussion

Implications of isotopic data

Neodymium isotopic compositions of wehrlite and pyroxenite samples are not indicative of significant crustal contamination. This is consistent with trace element ratios of these rocks that are similar to that of OIB. The elevated ε_{Nd} value (>4) of the gabbro sample may be due to derivation from a mantle source characterized by a modest enrichment in Sm (and elevated $^{143}Nd/^{144}Nd$), or possibly from mixing of magma from sources with variable $^{147}Nd/^{143}Nd$ values. Alternatively, hydrothermal alteration involving a fluid with an elevated $^{143}Nd/^{144}Nd$ ratio could also have lead to a small increase in the ε_{Nd} value. Osmium isotopic values also demand that the Jinbaoshan system was open during some stages. The elevated γ_{Os} (259 Ma) values of wehrlite samples from the Jinbaoshan ultramafic intrusion could be indicative of crustal contamination including a contaminant characterized by elevated $^{187}Os/^{188}Os$ values but low Re/Os ratios. Most sedimentary sulfides tend to have high Re/Os ratios (e.g., Lambert et al. 1998), so it is difficult to envision

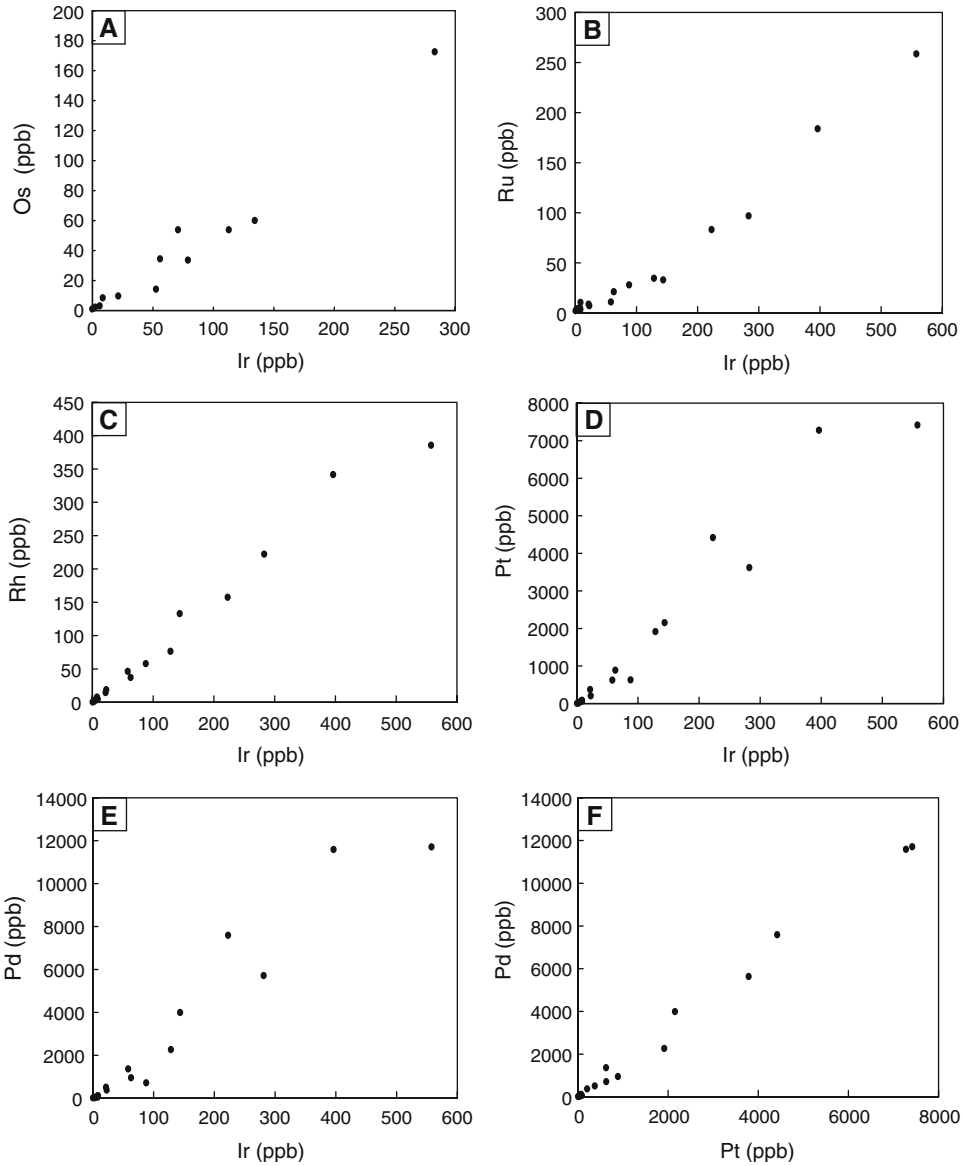

Fig. 9 Plots of Ir versus Os, Ru, Rh, Pt and Pd, and Pt versus Pd for the Jinbaoshan wehrlites

contamination related to assimilation of sedimentary material. This interpretation is also inline with the S isotopic values of the ores, which are near those considered to be normal for mantle-derived melts and which differ strongly from the values of pyrite in country rocks. Gangopadhyay and Walker (2003) and Puchtel et al. (2004) suggest that closed system behavior of Re in ultramafic systems is characterized by linear relations between Re and Al_2O_3, and Re and MgO. Although we do not have enough analyses of sulfide-poor samples for such an evaluation, the relatively low Re/Os ratios of all samples may be a function of the extensive hydrothermal alteration/serpentinization. The suprachondritic nature of the samples may be the result of hydrothermal processes which affected rocks that were initially chondritic in character. The apparent decoupling of the Sm–Nd and Re–Os isotopic systems is most easily explained as a result of extensive Re loss during hydrothermal alteration.

The large range in the sulfur isotopic values of secondary pyrite may indicate that sulfur sources distinct from the mineralized igneous rocks contributed to the hydrothermal fluid. A more likely alternative is that local variations in oxidation state and the ratio of sulfate to sulfide in the hydrothermal fluid resulted in the crystallization of pyrite with widely varying $\delta^{34}S$ values (e.g. Ripley et al. 2005).

Trapped liquid content and composition

We have used the concentrations of Ce and Nb in the Emeishan low-Ti, high-MgO basalts analyzed by Xu

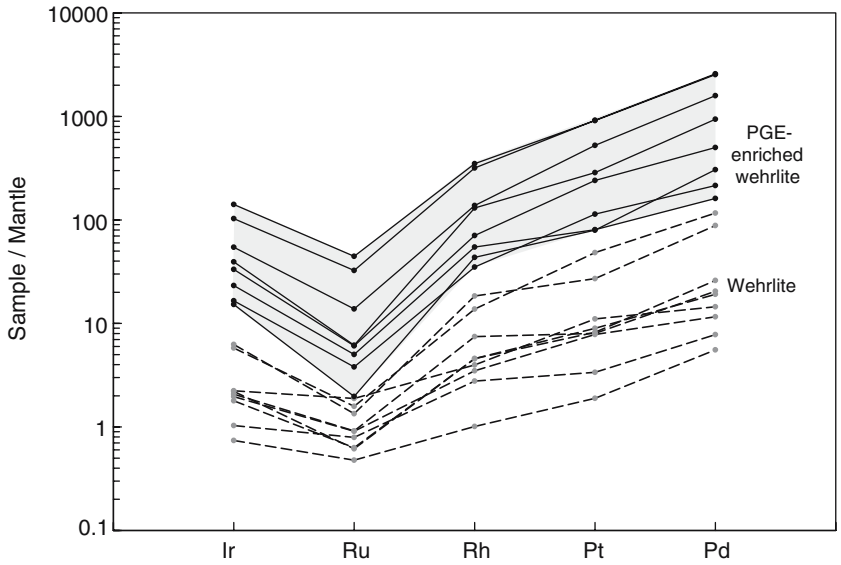

Fig. 10 Mantle-normalized patterns of platinum-group elements for the Jinbaoshan intrusive rocks and the Emeishan picrites. The mantle values are from Barnes and Maier (1999)

et al. (2001) to estimate the amounts of trapped liquid in the wehrlite samples. Our calculations indicate that most of the wehrlite samples represent mixtures of 20–40 wt% trapped liquid with 60–80 wt% olivine.

The compositions of trapped liquid in the Jinbaoshan wehrlites are estimated using the method of Chai and Naldrett (1992). The results are shown in Fig. 7d. Line E to F in the figure represents the FeO^{total}/MgO ratio of a liquid in equilibrium with olivine Fo84, the most Mg-rich olivine in the Jinbaoshan wehrlites. The Mg–Fe distribution coefficient ($K_D = (FeO/MgO)^{olivine}/(FeO/MgO)^{liquid}$, at% or wt% ratio) of 0.3 from Roeder and Emslie (1970) was used in the calculations. The ratio of FeO/FeO^{total} is assumed to be 0.9. This value is reasonable for an oxidation state close to the QFM buffer. Point A represents the compositions of olivine Fo84. Point B is the average compositions of wehrlites with <0.5 wt% S and <2 wt% Cr_2O_3. The average FeO^{total} value of the wehrlite samples was corrected for Fe_2O_3 in the trapped liquid portion using a FeO/FeO^{total} ratio of 0.9. The average values of ~70 wt% olivine and ~30 wt% trapped liquid (i.e., interstitial phases) in the wehrlites were used in the calculations. The values are consistent with the concentrations of incompatible elements in the samples (see below). Assuming that the wehrlites represent mixtures of olivine Fo84 with a coexisting liquid, the FeO and MgO contents in the liquid can be estimated by extrapolation of line A to B to intercept line E to F at point C (Fig. 7d), which gives 14 wt% FeO^{total} and 11 wt% MgO in the liquid. Compared to this liquid, the associated gabbroic rocks contain much lower MgO.

Table 4 Sulfur isotopes of sulfides from the Jinbaoshan deposit

Sample	Mineral	Rock type	$\delta^{34}S$
82-2a	Pyrrhotite	Disseminated ore	1.1
82-2b	Pyrrhotite	Disseminated ore	1.6
2H22a	Pyrrhotite	Disseminated ore	1.9
2H22b	Pyrrhotite	Disseminated ore	2.0
2H22c	Pyrrhotite	Disseminated ore	2.0
2H22d	Pyrrhotite	Disseminated ore	2.0
145-3a	Pyrrhotite	Disseminated ore	1.2
145-3b	Pyrrhotite	Disseminated ore	1.9
145-4a	Pyrrhotite	Disseminated ore	1.7
145-4b	Pyrrhotite	Disseminated ore	1.5
82-2	Chalcopyrite	Cp vein	0.6
145-4e	Chalcopyrite	Cp vein	2.8
145-3c	Chalcopyrite	Cp–Py vein	1.6
145-3d	Pyrite	Cp–Py vein	2.1
322-7	Pyrite	Disseminated ore	0.6
144a	Pyrite	Breccia sulfide ore	6.5
144b	Pyrite	Breccia sulfide ore	5.4
322-6a	Pyrite	Breccia sulfide ore	–23.0
322-6b	Pyrite	Breccia sulfide ore	–21.9
176-1	Pyrite	dolomite xenolith	18.5
176-3	Pyrite	Dolomite xenolith	18.6
39J-2a	Pyrite	Py vein in dolomite footwall	11.7
39J-2b	Pyrite	Py vein in dolomite footwall	12.1

Cp chalcopyrite, *py* pyrite

Relations of different rock units

The contrasting mineral and chemical compositions between the Jinbaoshan ultramafic intrusion and associated gabbros presented above are consistent with the interpretation that the gabbroic rocks are early intrusive phases that have no genetic link to the Jinbaoshan ultramafic intrusion. Minor pyroxenite in the margins of the wehrlite unit possibly formed by liquid

Table 5 Neodymium isotopic compositions of whole rocks from the Jinbaoshan intrusion and associated gabbro

Sample	Rock unit	Sm (ppm)	Nd (ppm)	$^{147}Sm/^{144}Nd$	$^{143}Nd/^{144}Nd$	$^{143}Nd/^{144}Nd$ (259 Ma)	ε_{Nd} (259 Ma)
145-3R	Mineralized wehrlite	0.783	3.8	0.1232	0.512526 ± 15	0.512317	0.24
JB19	Mineralized wehrlite	1.363	6.6	0.1247	0.512523 ± 11	0.512312	0.14
1309-2	Wehrlite	1.274	6.3	0.1231	0.512554 ± 19	0.512346	0.79
B33	Wehrlite	1.648	7.2	0.1394	0.512537 ± 11	0.512301	–0.09
B2	Pyroxenite	2.502	12.1	0.1255	0.512514 ± 14	0.512301	–0.07
JBB-3	Gabbro	6.203	22.0	0.1710	0.512810 ± 12	0.512520	4.19

ε_{Nd} is the derivation in parts per 10,000 of the initial ratio from that of a chondritic reservoir at the crystallization age of 259 Ma

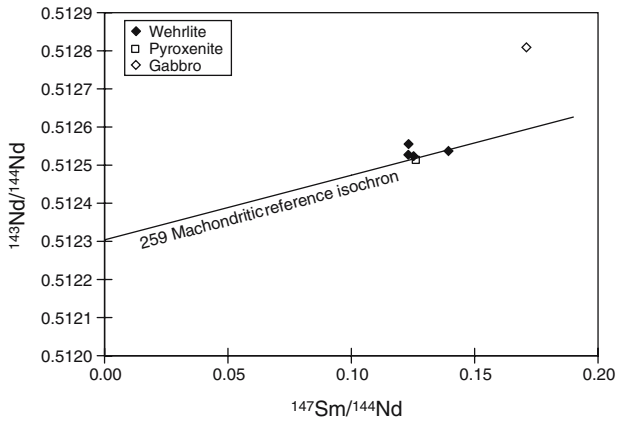

Fig. 11 Plot of $^{147}Sm/^{144}Nd$ versus $^{143}Nd/^{144}Nd$ of whole rock samples from the Jinbaoshan intrusive rocks with a chondritic 259 Ma reference line

expelled from the wehrlite unit in response to flow differentiation of an olivine-bearing magma or compaction during solidification. This interpretation is consistent with the similar ε_{Nd} values and trace and rare earth element patterns between wehrlite and pyroxenite units.

Major and trace element compositions suggest that the Jinbaoshan wehrlites contain 40–60% cumulus olivine. If the associated pyroxenite unit, which accounts for ~10% of the intrusion, is added as a liquid component, the intrusion contains 30–50% cumulus olivine. These values are 10–20% higher than the abundance of olivine phenocrysts in the associated picrites in the ELIP. It is difficult for a crystal mush comprising >30% crystals to travel for a long distance because such a mush would behave like a solid instead of a liquid (Marsh 1981; Brophy 1991). Therefore, we suggest that the enrichment of olivine in the Jinbaoshan intrusion was due to reaction of passing magma with partially solidified rocks (e.g. Keleman et al. 1992) during which plagioclase was selectively dissolved by the passing magma. This is consistent with depletion of Sr and Eu in the wehrlites that are poor in plagioclase.

Sulfide and PGE enrichment

The average contents of trapped liquids in the Jinbaoshan wehrlites are estimated to be less than 30%. The maximum solubility of S in the trapped liquids estimated using the equation of Li and Ripley (2005) is <1,200 ppm. If cumulus sulfide is not present, the amount of S in the Jinbaoshan wehrlites would be less than 400 ppm. ''Normal'' wehrlites as well as PGE-enriched wehrlites of the Jinbaoshan intrusion contain as least twice this value, indicating the presence of cumulus sulfide. We propose that the excessive sulfide in the intrusion was brought in by ascending magma in the form of immiscible sulfide droplets.

Table 6 Osmium isotopic compositions of whole rocks from the Jinbaoshan intrusion

Sample	Rock type	Re (ng/g)	Os (ng/g)	$^{187}Re/^{188}Os$	$^{187}Os/^{188}Os$	$^{187}Os/^{188}Os$ (259 Ma)	γ_{Os} (259 Ma)
145-3s	Disseminated sulfide	14.25	202.50	0.338	0.1533 ± 14	0.1519	20.71
145-3V	Sulfide vein	1.91	28.66	0.319	0.1552 ± 108	0.1538	22.28
322-6V	Sulfide vein	1.05	14.41	0.348	0.2252 ± 26	0.2237	77.82
145-3R	Disseminated sulfide	7.91	203.40	0.186	0.1542 ± 19	0.1534	21.94
322-6R	Wehrlite	0.95	3.32	1.369	0.1871 ± 32	0.1812	44.02
JB19	Wehrlite	0.34	1.45	1.124	0.2069 ± 62	0.2020	60.60
1309-2	Wehrlite	0.38	2.01	0.912	0.2029 ± 34	0.1990	58.15
B33	Wehrlite	0.05	1.35	0.186	0.1834 ± 84	0.1826	45.15

γ_{Os} is the percent deviation of the initial ratio from that of a chondritic reservoir at the crystallization age of 259 Ma

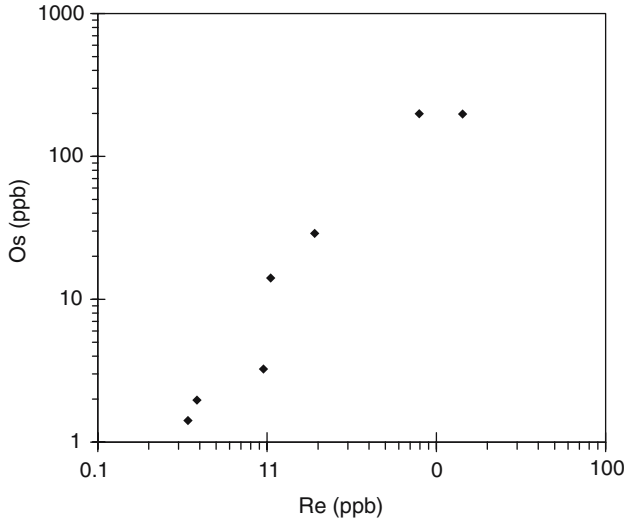

Fig. 12 Plot of Re versus Os of whole rock samples from the Jinbaoshan intrusion

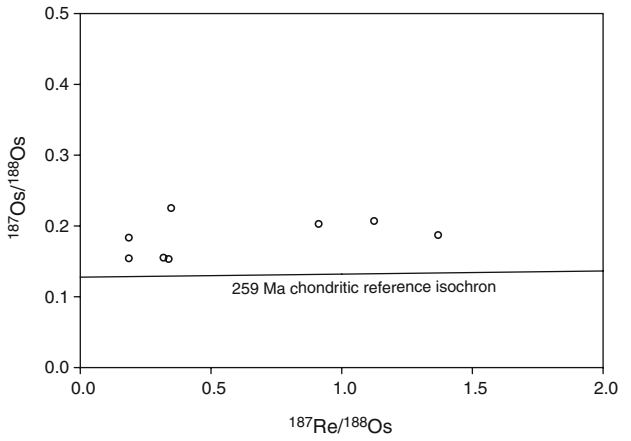

Fig. 13 Plot of $^{187}Re/^{188}Os$ versus $^{187}Os/^{188}Os$ of whole rock samples from the Jinbaoshan intrusion with a chondritic 259 Ma reference line

Sulfide saturation in mafic magma may be induced by fractional crystallization, magma mixing and crustal contamination (see a review by Li and Ripley 2005). No clear evidence for magma mixing or crustal contamination is found in the Jinbaoshan intrusion. Thus, fractional crystallization is most likely the cause of sulfide saturation at Jinbaoshan. Textural relations indicate that chromite and olivine are early phases to crystallize in the Jinbaoshan intrusion. Crystallization of chromite and olivine not only increase the content of S but also reduce the solubility of S in the residual liquid, thereby trigger sulfide saturation (Li and Ripley 2005). The Jinbaoshan olivine is moderately fractionated (low Fo) as compared to most olivine phenocrysts in the Emeishan picrites. Depletion of Ni in the Jinbaoshan olivine is consistent with the interpretation that sulfide segregation took place at depth during early stages of olivine + chromite crystallization and that the Jinbaoshan olivine crystallized after initial sulfide segregation. Os and Ru are highly compatible in chromite (Righter et al. 2004). Ir is compatible in olivine (Brenan et al. 2005). The depletions of Os–Ir–Ru in the Jinbaoshan wehrlites are consistent with early olivine + chromite crystallization before sulfide segregation. We envision that some small sulfide droplets segregated at depth were transported by magma to the Jinbaoshan feeder system. Reaction of the sulfide liquids with new magma passing through the Jinbaoshan conduit further enriched PGE in the sulfide liquid.

Effect of hydrothermal alteration on PGE distribution

Mass balance calculations using mineral compositions and whole rock analyses indicate that pentlandite and millerite are the major hosts for Pd in the samples. In contrast, Pt occurs as discrete minerals with As, Te and Pd. The spatial association of these minerals with secondary silicates, magnetite and pyrite (Fig. 4b, c) suggest that hydrothermal alteration has affected the final distribution of Pt and Pd in the samples. Experimental work (see a review by Wood 2002) indicates that Pd is more mobile in aqueous fluids than is either Pt or Ir. Therefore, decoupling of these elements may occur during fluid–rock interaction.

Conclusions

1. The gabbroic rocks in the Jinbaoshan area are early intrusive phases that are not genetically related to the Jinbaoshan ultramafic intrusion.
2. The Jinbaoshan wehrlites represent residual assemblages formed by dissolution of plagioclase by passing magma in a dynamic conduit.
3. Sulfide saturation occurred at depth possibly due to olivine + chromite crystallization.
4. Immiscible sulfide droplets segregated at depth were transported by ascending magma to accumulate in the Jinbaoshan conduit where they reacted with new magma passing through the conduit to achieve high PGE concentrations.
5. The final distribution of PGE has been affected by alteration/serpentinization.

Acknowledgments We thank Jindong Qi and colleagues of the Third Geology Survey Team, Yunnan Bureau of Geology and Mineral Resources, China for their support during the fieldwork.

This study was supported by the Chinese Academy of Sciences (KZCX3-sw-125) and the National Science Foundation of China (40573020, 40473025 and 40534020). Research at Indiana University on the genesis of magmatic sulfide deposits has been supported by NSF grant EAR-0335131. Alan Boudreau and an anonymous reviewer provided thoughtful reviews of an earlier draft of the paper.

References

Ali JR, Lo CH, Thompson GM, Song XY (2004) Emeishan basalt Ar–Ar overprint ages define several tectonic events that affected the western Yangtze platform in the Mesozoic and Cenozoic. J Asian Earth Sci 23:163–178

Anders E, Grevesse N (1989) Abundances of the elements: meteoritic and solar. Geochim Cosmochim Acta 53:197–214

Barnes S-J, Maier WD (1999) The fractionation of Ni, Cu and the noble metals in silicate and sulfide liquids. In: Keays RR, Lesher CM, Lightfoot PC, Farrow CEG (eds) Dynamic processes in magmatic ore deposits and their application in mineral exploration, vol. 13. Geological Association of Canada Short Course pp 69–106

Brophy JG (1991) Composition gaps, critical crystallinity, and fractional crystallization in orogenic magmatic systems. Contrib Miner Petrol 109:173–182

Burchfiel BC, Chen Z, Liu Y, Royden LH (1995) Tectonics of the Longmenshan and adjacent regions, central China. Int Geol Rev 37:661–736

Boven A, Pasteelsa AP, Punzalana LE, Liu BJ, Luoa X, Zhang BW, Guo BZ, Hertogen CJ (2002) $^{40}Ar/^{39}Ar$ geochronological constraints on the age and evolution of the Permo-Triassic Emeishan volcanic province, Southwest China. J Asian Earth Sci 20:157–175

Brenan JM, MvDonough WF, Ash R (2005) An experimental study of the solubility and partitioning of iridium, osmium and gold between olivine and silicate melt. Earth Planet Sci Lett 237:855–872

Chai G, Naldrett AJ (1992) The Jinchuan ultramafic intrusion: cumulate of a high-Mg basaltic magma. J Petrol 33:277–303

Chung SL, Jahn BM (1995) Plume–lithosphere interaction in generation of the Emeishan flood basalts at the Permian–Triassic boundary. Geology 23:889–892

Du A, Wu SQ, Sun DZ, Wang SX, Makey R, Stein H, Morgan J, Malinovsky D (2004) Preparation and certification of Re–Os dating reference materials: molybdenite HLP and JDC. Geostand Geoanal Res 28:41–52

Fan WM, Wang YJ, Peng TP (2004) Ar–Ar and U–Pb geochronology of Late Paleozoic basalts in west Guangxi and its constraints on the eruption age of Emeishan basalt magmatism. Chin Sci Bull 49:2318–2327

Gangopadhyay A, Walker RJ (2003) Re–Os systematics of the ca. 2.7-Ga komatiites from Alexo, Ontario, Canada. Chem Geol 196:147–162

Guo F, Fan WM, Wang Y, Li C (2004) When did the Emeishan mantle plume activity start?: geochronological and geochemical evidence from ultramafic-mafic dikes in Southwestern China. Int Geol Rev 46:226–234

Jin Y, Shang J (2000) The Permian of China and its interregional correlation. In: Yin H, Dickins JM, Shi GR, Tong J (eds) Permian–Triassic evolution of Tethys and western Circum-Pacific: developments in Paleontology and Stratigraphy 18. Elsevier, Amsterdam, pp 71–98

Keleman PB, Dick HJB, Quick JE (1992) Formation of harzburgite by pervasive melt/rock in the upper mantle. Nature 358:635–641

Lambert DD, Foster JG, Frick LR, Ripley EM, Zientek ML (1998) Geodynamics of magmatic Cu–Ni–PGE sulfide deposits: new insights from the Re–Os isotopic system. Econ Geol 93:121–137

Li C, Ripley EM (2005) Empirical equations to predict the sulfur content of mafic magma at sulfide saturation and applications to magmatic sulfide deposits. Miner Depos 40:218–230

Ma YX, Ji XT, Li JC, Huang M, Min ZZ (2003) Mineral resources of Panzhihua, Sichuan Province, SW China. Chengdu University of Technology, pp 275

Marsh BD (1981) On the crystallinity, probability of occurrence, and rheology of lava and magma. Contrib Mineral Petrol 78:85–98

Puchtel IS, Humayum M, Campbell AJ, Sproule RA, Lesher CM (2004) Platinum-group element geochemistry of komatiites from the Alexo and Pyke Hill areas, Ontario, Canada. Geochim Cosmochim Acta 68:1361–1383

Qi L, Grégoire DC (2000) Determination of trace elements in twenty six Chinese geochemistry reference materials by inductively coupled plasma-mass spectrometry. J Geostand Geoanal 24:51–63

Qi L, Grégoire DC, Zhou M-F, Malpas J (2003) Determination Pt, Pd, Ru, and Ir in geological samples by ID-ICP-MS using sodium peroxide fusion and Te co-precipitation. Geochem J 37:557–565

Righter K, Campbell AJ, Humayun H, Hervig RL (2004) Partitioning of Ru, Rh, Pd, Re, Ir, and Au between Cr-bearing spinel, olivine, pyroxene and silicate melts. Geochim Cosmochim Acta 68:867–880

Ripley EM, Sarkar A, Li C (2005) Mineralogic and stable isotopic studies of hydrothermal alteration at the Jinchuan Ni–Cu deposit. Econ Geol 100:1349–1361

Roeder PL, Emslie RF (1970) Olivine–liquid equilibrium. Contrib Miner Petrol 29:275–289

Shirey SB, Walker RJ (1995) Carius tube digestion for low-blank rhenium–osmium analysis. Anal Chem 67:2136–2141

Song X-Y, Zhou M-F, Hou Z-Q, Cao Z-M, Wang Y-L, Li Y-G (2001) Geochemical constraints on the mantle source of the Upper Permian Emeishan continental flood basalts, southwestern China. Int Geol Rev 43:213–225

Song X-Y, Zhou M-F, Cao ZM, Sun M, Wang YL (2003) Ni–Cu–(PGE) magmatic sulfide deposits in the Yangliuping area, Permian Emeishan igneous province, SW China. Miner Depos 38:831–843

Studley SA, Ripley EM, Elswick ER, Dorais MJ, Fong J, Finkelstein D, Pratt LM (2002) Analysis of sulfides in whole rock matrices by elemental analyzer-continuous flow isotope ratio mass spectrometry. Chem Geol 192:141–148

Sun SS, McDonough WF (1989) Chemical and isotopic systematics in ocean basalt: implication for mantle composition and processes. In: Saunders AD, Norry MJ (eds) Magmatism in the Ocean Basins. Geological Society of London Special Publications 42:313–345

Wang CY, Zhou M-F, Zhao D (2005) Mineral chemistry of chromite from the Permian Jinbaoshan Pt–Pd-sulphide-bearing ultramafic intrusion in SW China, with petrogenetic implications. Lithos 83:47–66

Wang CY, Zhou M-F, Keays RR (2006) Geochemical constraints on the origin of the Permian Baimazhai mafic-ultramafic intrusion, SW China. Contrib Miner Petrol 152:309–321

Wood SA (2002) The aqueous geochemistry of the platinum-group elements with applications to ore deposits. In: Cabri LJ (eds) The geology, geochemistry, mineralogy and mineral beneficiation of PGE, vol. 54. Canadian Institute of Mining, Metallurgy and Petroleum Special, pp 211–250

Xiao L, Xu YG, Mei HJ, Zheng YF, He B, Pirajno F (2004) Distinct mantle sources of low-Ti and high-Ti basalts from the western Emeishan large igneous province, SW China: implications for plume–lithosphere interaction. Earth Planet Sci Lett 228:525–546

Xu YG, Chung SL (2001) Emeishan Large Igneous Province: Evidence for mantle plume activity and melting conditions (in Chinese with English abstract). Geochimica 30:1–9

Xu YG, Chung SL, Jahn BM, Wu GY (2001) Petrological and geochemical constraints on the petrogenesis of the Permo-Triassic Emeishan Flood basalts in southwestern China. Lithos 58:145–168

Xu YG, He B, Chung SL, Menzies MA, Frey FA (2004) Geologic, geochemical, and geophysical consequences of plume involvement in the Emeishan flood-basalt province. Geology 32:917–920

Yang TX (1989) The Jinbaoshan Pt–Pd deposit in Midu County, Yanan, China (in Chinese). Unpublished report of the 3rd Geological Team, Yanan Province, pp 236

Yin H, Huang S, Zhang K, Hansen HJ, Yang F, Ding M, Bie X (1992) The effects of volcanism of the Permo-Triassic mass extinction in South China. In: Sweet WC, Yang ZY, Dickins JM, Yin HF (eds) Permo-Triassic events in the Eastern Tethys: stratigraphy, classification, and relations with the Western Tethys. World and Regional Geology, vol. 2. Cambridge University Press, Cambridge, pp 146–157

Zhang HF, Sun M, Lu Fx, Zhou XH, Zhou M-F, Liu YS, Zhang GH (2001) Moderately depleted lithospheric mantle underneath the Yangtze Block: evidence from a garnet lherzolite xenolith in the Dahongshan kimberlite. Geochem J 35:315–331

Zhong H, Zhou XH, Zhou M-F, Sun M, Liu BG (2002) Platinum-group element geochemistry of the Hongge Fe–V–Ti deposit in the Pan–Xi area, southwestern China. Miner Depos 37:226–239

Zhong H, Yao Y, Hu SF, Zhou XH, Liu BG, Sun M, Zhou M-F, Viljoen MJ (2003) Trace-Element and Sr–Nd Isotopic Geochemistry of the PGE-Bearing Hongge Layered Intrusion, Southwestern China. Int Geol Rev 45:371–382

Zhou M-F, Maplas J, Song XY, Robinson PT, Sun M (2002a) A temporal link between the Emeishan large igneous province (SW China) and the end-Guadalupian mass extinction. Earth Planet Sci Lett 196:113–122

Zhou M-F, Yan DP, Kennedy AK, Li YQ, Ding J (2002b) SHRIMP zircon geochronological and geochemical evidence for Neoproterozoic arc-related magmatism along the western margin of the Yangtze Block, South China. Earth Planet Sci Lett 196:51–67

Zhou M-F, Yang ZX, Song X-Y, Lesher CM, Keays RR (2002c) Magmatic Ni–Cu–(PGE) sulphide deposits in China. In: Cabri LJ (eds) The geology, geochemistry, mineralogy and mineral beneficiation of platinum-group elements. Canadian Institute of Mining, Metallurgy and Petroleum Special volume 54:459–481

Zhou M-F, Robinson PT, Lesher CM, Keays RR, Zhang C-J, Malpas J (2005) Geochemistry, petrogenesis and metallogenesis of the Panzhihua gabbroic layered intrusion and associated Fe–Ti–V oxide deposit, Sichuan Province, SW China. J Petrol 46:2253–2280

Zhou M-F, Ma Y, Yan D-P, Xia X, Zhao J-H, Sun M (2006) The Yanbian Terrane (Southern Sichuan Province, SW China): a Neoproterozoic arc assemblage in the western margin of the Yangtze block. Precambrian Res 144:19–38